Journal of Alloys and Compounds 731 (2018) 364–368

Contents lists available at ScienceDirect

Journal of Alloys and Compounds

journal homepage: http://www.elsevier.com/locate/jalcom

Hard three-dimensional BN framework with one-dimensional metallicity

Mei Xiong, Kun Luo, Yilong Pan, Lingyu Liu, Guoying Gao, Dongli Yu, Julong He*, Bo Xu, Zhisheng Zhao**

State Key Laboratory of Metastable Materials Science and Technology, Yanshan University, Qinhuangdao, Hebei 066004, China

ARTICLE INFO

Article history:
Received 6 July 2017
Received in revised form
25 September 2017
Accepted 27 September 2017
Available online 28 September 2017

Keywords:
First-principles calculations
Boron nitride
Electronic properties
One-dimensional metallicity
Low energy
Hard material

ABSTRACT

Carbon can be metal, semiconductor or insulator depending on its structures, and its conductivity can be one-dimensional (1D), 2D, and 3D correspondingly. Boron Nitride (BN) is isoelectronic to carbon, but one prominent difference between the two systems is their electronic properties. For many years, the synthesized and predicted BN allotropes were always insulators, irrespective of their structures. In this paper, with the help of structures searching based on first-principles calculations, a sp^2/sp^3-hybridized metallic monoclinic 3D BN (*M*-BN) structure is proposed. *M*-BN can be viewed as puckered hexagonal-BN (h-BN) layers bucked by partial sp^3 B–N bonds. The electronic property analysis revealed that the metallicity of *M*-BN is attributed to the delocalized 2*p* electrons of the sp^2 B and N atoms. The metallic B atoms and N atoms are aligns in two arrays along a 1D axial direction, resulting in the unusual 1D dual-threaded conduction in 3D *M*-BN structure. The enthalpy calculation have revealed that *M*-BN is the most energetically favorable structure among the predicted metallic BN structures so far, and it might be obtained via compressing layered h-BN precursor theoretically. Due to the 3D strong framework, *M*-BN has an estimated Vickers Hardness of 33.7 GPa, indicating it is a potential hard material with novel 1D conduction.

1. Introduction

Boron nitride is considered an intriguing compound, and has thus been studied for many years. There are four basic experimentally BN frameworks, including hexagonal BN (h-BN), rhombohedral BN (r-BN), wurtzite BN (w-BN), and cubic BN (c-BN). Since h-BN has been successfully synthesized, one of the topics in BN system is the exploration of novel BN structures. In the early years, studies were focused on high-pressure phase transitions between layered sp^2-hybridized (h-BN/r-BN) and sp^3-hybridized (w-BN/c-BN) phases [1–6]. In the past two decades, researchers have attempted to synthesize novel BN polymorphs via chemical methods and explore their potential applications. Some examples are the synthesized 1D BN nanotubes (BNNTs) for biomedicine applications, 2D BN nanosheets and BN nanoribbons for optoelectronics, or 3D porous BN architectures with high thermal conductivity [7–10]. In terms of their electronic applications, these synthesized BN compounds are always considered semiconductors/insulators, while reports on BN compounds used as conductive materials are scarce. However, it has been reported that BNNRs can be transformed into metallic by an external electric field [11]. Thus, searching for BN phases with intrinsic metallicity is still attracting the attention of researchers. Owing to the mechanical stability of 3D frameworks, 3D metallic BN has been highly anticipated and would have exciting applications in electronic devices.

Due to the ability of B and N atoms to form *sp*-, sp^2-, and sp^3-hybridizations, BN compounds can theoretically exhibit a variety of frameworks. In recent years, with the aid of first-principles calculations, a series of novel BN structures have been proposed [12–32]. Most of them are wide band gap semiconductors, including some superhard structures [15,20–23], 3D BN nanotubes and nanoribbon polymers [16,18], and 3D fully sp^2-hybridized structures [23,24]. This situation changed since 2013 when 3D metallic BN structures were predicted in three studies [29–31]. Unfortunately, one of the four structures, i.e. T-B_3N_3, was proven to be mechanically unstable in a subsequently study [33], and the four structures had also relatively high ground-state energies. These results prompt us to

* Corresponding author.
** Corresponding author.
E-mail addresses: hjl@ysu.edu.cn (J. He), zzhao@ysu.edu.cn (Z. Zhao).

https://doi.org/10.1016/j.jallcom.2017.09.307
0925-8388/

further explore metallic BN allotropes with high thermodynamical and mechanical stabilities, which may possibly be synthesized in the future, as was the case of the theoretically predicted BNNTs in 1994 that were later prepared by experimental scientists in 1995 [34,35]. Moreover, the metallicity in different dimensions (1D, 2D, and 3D) would potentially result in a wide variety of electronic properties and applications. Particularly, the unusual 1D or 2D conduction in 3D frameworks would be worth pursuing, due to its advantageous combination of both novel electronic properties and robust mechanical stability.

In this study, a 3D sp^2/sp^3-hybridized BN allotrope with novel 1D metallicity is theoretically proposed. This BN form has a monoclinic structure, and thereby has been denoted as *M*-BN. *M*-BN is mechanically and dynamically stable at zero pressure. It is the most energetically stable allotrope among the proposed metallic BN structures so far, and its energy is comparable to some pure sp^3 BN structures previously proposed. Due to the structural similarity, *M*-BN may be obtained by compressing layered BN precursor through partial sp^3 buckle, like the transition from graphite to diamond. Furthermore, we also study the origin of unusual 1D metallicity and excellent mechanical performance for this hybridized BN structure.

2. Computational methods

The BN structural searching was executed through the well-developed CALYPSO code [36], which is based on *ab inito* particle-swarm optimization. It was conducted up to 12 BN formulas per unit cell. Further structural optimizations, electron orbits and elastic properties of the pre-screened structures were performed using the CASTEP code based on density functional theory (DFT) [37]. The plane wave energy-cutoff is set as 330 eV with ultra-soft pseudopotential, which was chosen to achieve the accuracy of total energy convergence of 1–2 meV per atom [38]. The local density approximation (LDA) functional of Ceperley and Alder parameterized by Perdw and Zunger (CA-PZ) was used for describe the electron-electron exchange interaction [39,40]. The Monkhorst-Pack grids for Brillouin zone sampling [41] was generated by $2\pi \times 0.04$ Å^{-1} *k*-point separation. Phonon dispersion spectra were calculated by finite displacement method in the CASTEP code by using primitive cell, and the unit cell was used to calculate elastic constants, bulk and shear modulus, and 0.003 was chosen as the applied maximum strain amplitude during process. The band structure was calculated by the HSE06 hybrid functional [42] as implemented in VASP code [43]. The used convergence plane wave cutoff energy was 550 eV, and the Monkhorst-Pack *k* mesh of $13 \times 13 \times 9$ for electronic property calculations.

3. Results and discussion

3.1. Structural configuration

The configuration of the predicted crystal structure is shown in Fig. 1 with different views. The structure has a monoclinic symmetry (*Cm* space group, No. 8), and thus has been denoted as *M*-BN hereafter. The fully relaxed lattice constants of *M*-BN structure are $a = 8.18$ Å, $b = 2.58$ Å, $c = 6.45$ Å, and $\beta = 133.3°$ at zero pressure. As shown in Fig. 1a and b, there are four inequivalent B and four inequivalent N atoms in per unit cell. The B atoms are colored in dark yellow, occupies the B1 (−0.495, −0.5, −0.728), B2 (−0.202, −0.5, −0.185), B3 (−0.133, 0, 0.53), B4 (−0.836, 0, −0.944), respectively. The N atoms are colored in blue, occupies the N1 (−0.895, 0, −0.215), N2 (−0.686, −0.5, −0.751), N3 (−0.255, −0.5, −0.467), N4 (−0.048, 0, 0.0026), respectively. In Fig. 1a, one can identify that B1 and N1 atoms are sp^2-hybridized, the other atoms are sp^3-hybridized. Fig. 1c shows, the *M*-BN can be viewed as puckered h-BN layers interlinked via sp^3 B–N bonds, the layered blocks are colored as rectangles in different colors. Due to the partial sp^3 bonding, *M*-BN has a density of 3.32 g/cm^3, lower than that of pure sp^3 hybridized c-BN (3.46 g/cm^3).

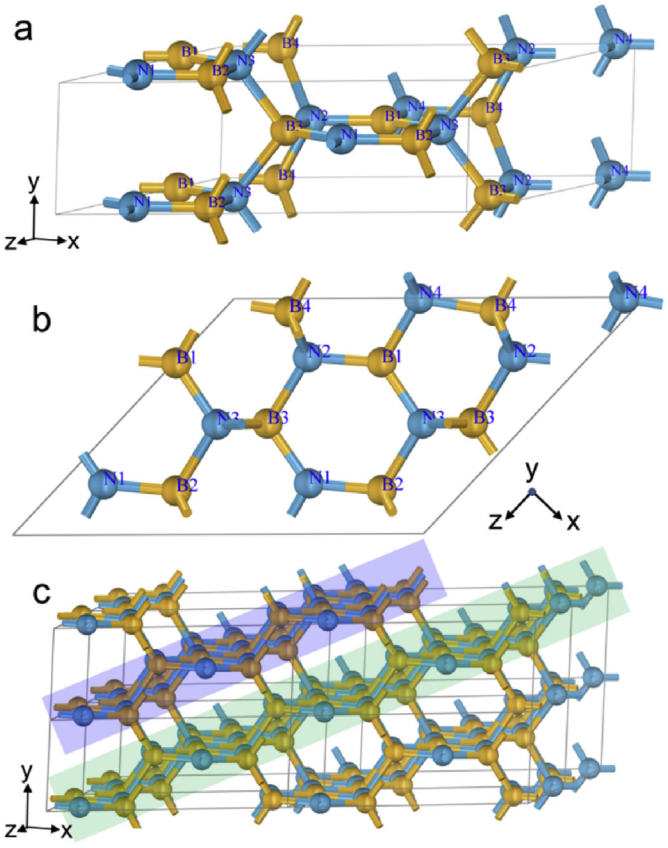

Fig. 1. Configurations of *M*-BN. The blocks marked with blue and green rectangles stand for the puckered h-BN layers. (For interpretation of the references to colour in this figure legend, the reader is referred to the web version of this article.)

3.2. Dynamical stability

The phonon spectra were calculated to study the dynamical stability of *M*-BN. We plotted the phonon dispersion curves of *M*-BN at 0 GPa and 40 GPa in Fig. 2, the sequence of high-symmetry

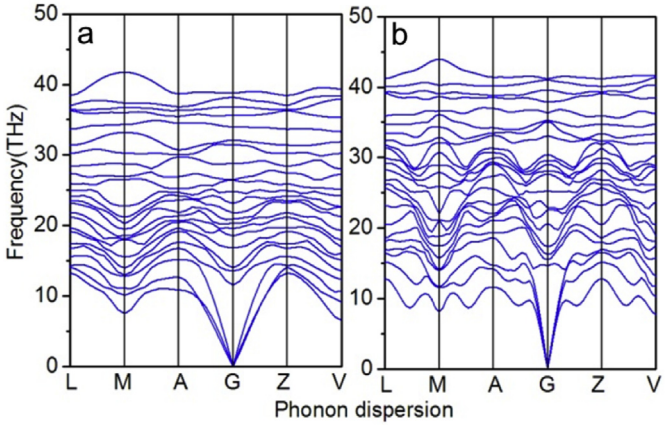

Fig. 2. Phonon dispersion curves of *M*-BN at (a) 0 GPa and (b) 40 GPa.

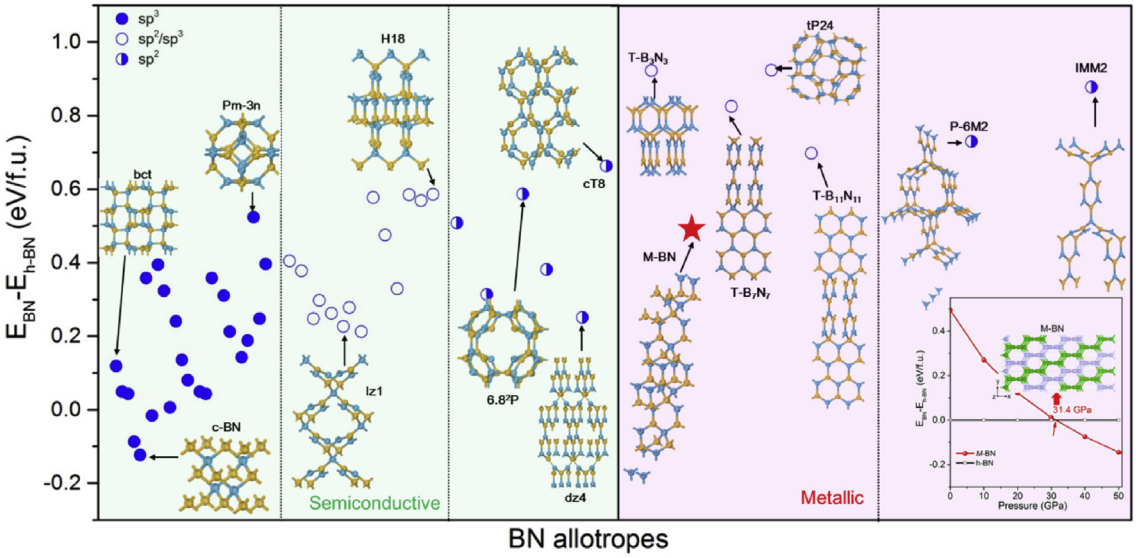

Fig. 3. Relative enthalpy for BN allotropes, including theoretical metallic BN [29–31] and proposed semiconductive BN [12,14–16,20–25,27,28,32]. The inset shows enthalpy of *M*-BN as a function of pressure relative to h-BN. *M*-BN is plotted with unit blocks in different colors, to show the structural features clearly (analogously to those Fig. 1c). (For interpretation of the references to colour in this figure legend, the reader is referred to the web version of this article.)

K-points in Brillouin zone is set as: L (−0.5, 0, 0.5)→M (−0.5, −0.5, 0.5)→A (−0.5, 0, 0)→G (0, 0, 0)→Z (0, −0.5, 0.5)→V (0, 0, 0.5). There are no imaginary frequencies in the whole Brillouin zone, indicating *M*-BN is dynamic stable at 0 (Fig. 2a) and 40 GPa (Fig. 2b).

3.3. Thermodynamic stability

To investigate the thermodynamic stability of *M*-BN, we calculated the relative enthalpy at ambient pressure with respect to other BN allotropes, including c-BN, w-BN and other 48 recently predicted BN structures, the results are shown in Fig. 3. Most of these BN structures are semiconductors/insulators, except the metallic structures predicted in three recent studies. In order to facilitate the comparison, semiconductive (left panel) [12,16,18,20–25,32] and metallic BN structures (right panel) [29–31] were classified as fully sp^2, fully sp^3 and mixed sp^2/sp^3 hybridizations. All the above hybridization forms can be found among the semiconductive BN allotropes, such as bct-BN [12], H18-BN [23], lz1-BN [16] and dz4-BN [16]. However, for the metallic BN structures, there are no fully sp^3 hybridized, but fully sp^2 and mixed sp^2/sp^3 identified structures predicted so far. The diversity of semiconductive BN frameworks affords widely ranging enthalpy values. Fig. 3 shows the energy of *M*-BN is comparable to that of certain semiconductive BN structures, such as the fully sp^3 $Pm\bar{3}n$-BN [32], which is possible to be synthesized experimentally [18,32]. Among the metallic BN structures, *M*-BN is the most energetically favorable phase. Therefore, the favorable energy of *M*-BN is an advantage toward its potential experimental synthesis. Moreover, the inset shows the enthalpy of the *M*-BN allotrope as a function of pressure compared to that of h-BN. *M*-BN is more energetically favored than h-BN at pressures above 31.4 GPa; it can thus be concluded that a high-pressure phase transition from h-BN to *M*-BN may happen at this point.

3.4. Mechanical stability

We calculated the elastic constants to test the mechanical stability of this structure. The calculated elastic constants of *M*-BN are C_{11}, C_{22}, C_{33}, C_{44}, C_{55}, C_{66}, C_{12}, C_{13}, C_{15}, C_{23}, and C_{35}. The correspondingly values (GPa) are 937.8, 383.0, 990.3, 151.6, 388.2, 170.9, 144.1, 127.9, −34.0, 90.8, and 18.1 respectively. The mechanical stability criteria of monoclinic structures are as follows [44]:

$$C_{ii} > 0,\ (\mathrm{i} = 1 - 6),$$

$$[C_{11} + C_{22} + C_{33} + 2(C_{12} + C_{13} + C_{23})] > 0,$$

$$\left(C_{33}C_{55} - C_{35}^2\right) > 0,$$

$$\left(C_{44}C_{66} - C_{46}^2\right) > 0,$$

$$(C_{22} + C_{33} - 2C_{23}) > 0,$$

$$\left[C_{22}\left(C_{33}C_{55} - C_{35}^2\right) + 2C_{23}C_{25}C_{35} - C_{23}^2C_{55} - C_{25}^2C_{33}\right] > 0,$$

$$\left\{\begin{array}{l} 2[C_{15}C_{25}(C_{33}C_{12} - C_{13}C_{23}) + C_{15}C_{35}(C_{22}C_{13} - C_{12}C_{23}) + C_{25}C_{35}(C_{11}C_{23} - C_{12}C_{13})] \\ -\left[C_{15}^2\left(C_{22}C_{33} - C_{23}^2\right) + C_{25}^2\left(C_{11}C_{33} - C_{13}^2\right) + C_{35}^2\left(C_{11}C_{22} - C_{12}^2\right)\right] + C_{55}g \end{array}\right\} > 0.$$

where $g = C_{11}C_{22}C_{33} - C_{11}C_{23}^2 - C_{22}C_{13}^2 - C_{33}C_{12}^2 + 2C_{12}C_{13}C_{23}$. Obviously, the elastic constants are satisfying the criteria, so *M*-BN structure is mechanically stable.

3.5. Electronic property

The screened hybrid functional HSE06 [42] is more accurate than LDA functional, in describing the exchange-correlation energy of electron in solids. Therefore, we calculated the band structure (Fig. 4a and b) of *M*-BN with the HSE06 functional. The results show that there are two bands crossing the Fermi level at L, Z (marked with red symbol line), M and V (marked with dark green symbol line), indicating *M*-BN is a metallic structure.

To explore the conductive mechanism of *M*-BN, the partial density of states (PDOS) of each atom has been calculated. The results show that both of the *p* orbital of sp^2 hybridized B1 and N1 atoms are contributes to the electronic states around the Fermi level (Fig. 4c). Fig. 4d–f plotted the electron orbits originated from the bands crossing the Fermi level to reveal the conductive network of *M*-BN. Fig. 4e shows the conducting channels in a view of the whole structure, the details of electron orbits in blue frame with different views are show in Fig. 4d and f. As show in Fig. 4d, owing to the short distance between B1 atoms from adjacent layers (2.58 Å), the electron orbits along *y* axis from sp^2 hybridized B1 atoms are linked together, resulting in a connected conductive pathway along *y* axis with π bonds. The orbits of N1 atoms along *y* axis are in the same situation as B1 atoms. Meanwhile, Fig. 4f shows there are no overlapped orbits between any conductive atoms in the *x*-*z* plane, indicating the interruption of conductivity. Noteworthy, in *M*-BN structure the distance between B1 and N1 atoms of a hexagonal ring is 2.81 Å, which is quite close to the value of B atom and its second-neighbor N atom (2.89 Å) in a h-BN layer. Therefore, it is reasonable for *M*-BN that the channels formed by B1 and N1 atoms are interrupted in the *x*-*z* plane just like the situation in h-BN. The particularly architecture afford the unique 1D dual-threaded conduction of *M*-BN structure. Notably, this unique 1D conducting behavior of *M*-BN is different from the T-B_3N_3 structure predicted in previously study [29]. The metallicity of T-B_3N_3 is originates from the sp^2 hybridized B atoms; a pyramid-like charge distribution is formed by the four nearest B atoms in this framework.

3.6. Hardness

Finally, the theoretical Vickers hardness of *M*-BN phases was calculated. In this paper, due to the metallicity of this covalent compound, the theoretical Vickers hardness is derived from the theoretical model proposed by Guo et al. [45] which depicted as

$$H_v(GPa) = 350(N_e)^{2/3}(d)^{-2.5}e^{-1.191f_i - 32.2(f_m)^{0.55}},$$

where N_e is the valance electron density, d is the bond length (Å), f_i is the Phillips iconicity and we used 0.256 for all B–N bonds, f_m is the metallic factor, for a μ-type bond,

$$f_m^\mu = \left[\frac{n_A^\mu}{N_{MA}} + \frac{n_B^\mu}{N_{MB}}\right] \Big/ n_e^\mu,$$

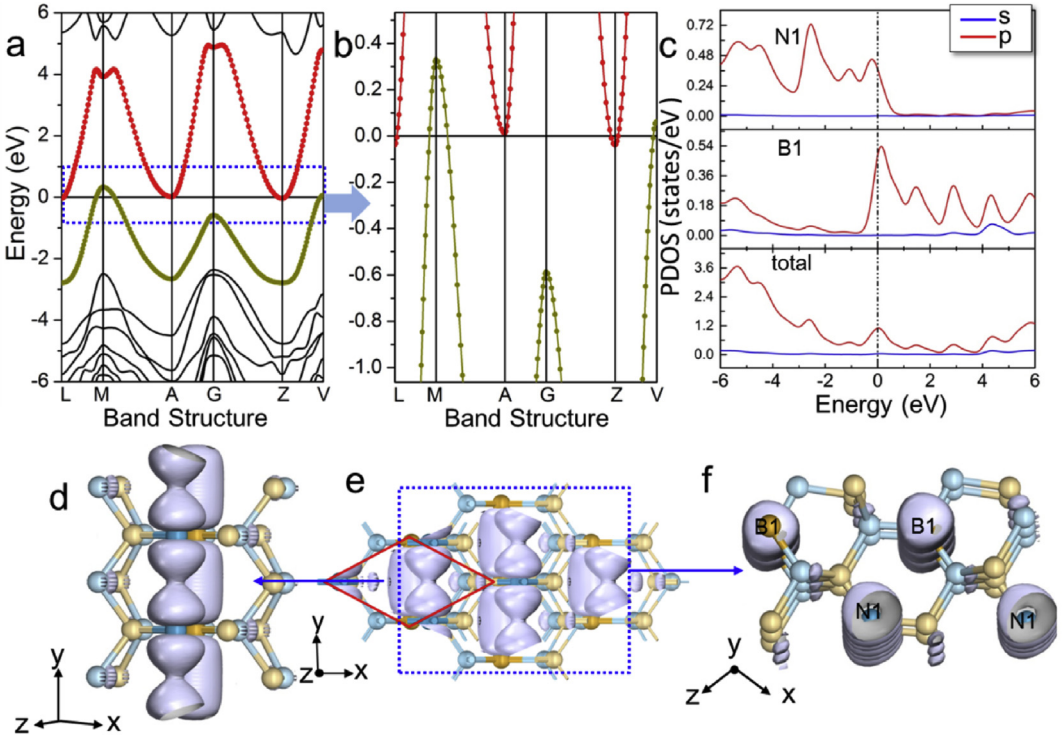

Fig. 4. Electronic properties of *M*-BN. (a) Band structure, the red and dark green lines are the bands across the Fermi level, and a magnified image in the blue frame is plotted in (b); (c) partial DOS of total structure, B1 atoms and N1 atoms; (d)–(f) electron orbits of *M*-BN, (e) electron orbits of *M*-BN with a whole structure view, red frame stands for a primitive cell; (d) the electron orbits of B1 atoms (similar with N1 atoms) from adjacent layers are linked each other along *y* axis; (f) the conducting channels in x-z plane are interrupted, resulting in the linear conduction of *M*-BN. The isosurface value is 0.1. The dark yellow and blue balls stand for B1 and N1 atoms, respectively; and the lighter ones stand for sp^3-hybridized atoms. (For interpretation of the references to colour in this figure legend, the reader is referred to the web version of this article.)

$n_A^{\mu}(n_B^{\mu})$ stands for the thermally excited electron number of atom A (B) in the μ-type bond, N_{MA} (N_{MB}) stands for the metallic component chemical bonds number around atom A (B), the number of valance electrons of per μ-type bond n_e^{μ} is depicted as:

$$n_e^{\mu} = \left[\frac{Z_A^{\mu}}{N_{CA}} + \frac{Z_B^{\mu}}{N_{CB}}\right],$$

where Z_A^{μ} (Z_B^{μ}) is the valance electron number of A (B) atom, and N_{CA} (N_{CB}) is the coordination number of A (B) atom. The calculated Vickers hardness of *M*-BN is 33.7 GPa. We compared the calculated hardness value by adopting the Chen's formula [46], which depicted as

$$H_v(GPa) = 2\left(G^3/B^2\right)^{0.585} - 3$$

and the bulk modulus (B) and shear modulus (G) of *M*-BN structure are 309.2 GPa and 246.3 GPa respectively. The result calculated by this formula is 35.4 GPa, the two values are close to each other, so the *M*-BN is considered as a hard framework.

4. Conclusions

In summary, we have proposed a novel hard metallic BN allotrope; it is a sp^2/sp^3 hybridized structure, named as *M*-BN. The energy of *M*-BN is energetically more favorable than the other predicted metallic BN structures so far, and is comparable to some other predicted semiconductive BN structures. The electronic band structure, density of states and electron orbits studies has shown that *M*-BN has 1D conduction. This conduction is different from the 3D conduction of T-B_3N_3 [29] and 2D conduction of modified BNNRs [11]. We expect that such novel 1D conduction in this 3D BN allotrope with robust mechanical stability will have promising applications in nanoelectronic devices and open new prospects for BN compounds and their electronic features.

Acknowledgments

This work is supported by National Science Foundation of China (51421091, 51332005, 51472213, and 51525205).

References

[1] R.H. Wentorf Jr., Cubic form of boron nitride, J. Chem. Phys. 26 (1957) 956.
[2] F.P. Bundy, R.H. Wentorf, Direct transformation of hexagonal boron nitride to denser forms, J. Chem. Phys. 38 (1963) 1144–1149.
[3] Q. Johnson, A.C. Mitchell, First X-ray diffraction evidence for a phase transition during shock-wave compression, Phys. Rev. Lett. 29 (1972) 1369–1371.
[4] F.R. Corrigan, F.P. Bundy, Direct transitions among the allotropic forms of boron nitride at high pressures and temperatures, J. Chem. Phys. 63 (1975) 3812–3820.
[5] H. Sumiya, T. Iseki, A. Onodera, High pressure synthesis of cubic boron nitride from amorphous state, Materials research bulletin, Mater. Res. Bull. 18 (1983) 1203–1207.
[6] Y. Tian, B. Xu, D. Yu, Y. Ma, Y. Wang, Y. Jiang, W. Hu, C. Tang, Y. Gao, K. Luo, Z. Zhao, L.M. Wang, B. Wen, J. He, Z. Liu, Ultrahard nanotwinned cubic boron nitride, Nature 493 (2013) 385–388.
[7] N.G. Chopra, R.J. Luyken, K. Cherrey, V.H. Crespi, M.L. Cohen, S.G. Louie, A. Zettl, Boron nitride nanotubes, Science 269 (1995) 966–967.
[8] C. Zhi, Y. Bando, C. Tang, H. Kuwahara, D. Golberg, Large-scale fabrication of boron nitride nanosheets and their utilization in polymeric composites with improved thermal and mechanical properties, Adv. Mater. 21 (2009) 2889–2893.
[9] H. Zeng, C. Zhi, Z. Zhang, X. Wei, X. Wang, W. Guo, Y. Bando, D. Golberg, "White graphenes": boron nitride nanoribbons via boron nitride nanotube unwrapping, Nano Lett. 10 (2010) 5049–5055.
[10] X. Zeng, Y. Yao, Z. Gong, F. Wang, R. Sun, J. Xu, C.P. Wong, Ice-templated assembly strategy to construct 3D boron nitride nanosheet networks in polymer composites for thermal conductivity improvement, Small 11 (2015) 6205–6213.
[11] A. Lopez-Bezanilla, J. Huang, H. Terrones, B.G. Sumpter, Boron nitride nanoribbons become metallic, Nano Lett. 11 (2011) 3267–3273.
[12] B. Wen, J. Zhao, R. Melnik, Y. Tian, Body-centered tetragonal B2N2: a novel sp3 bonding boron nitride polymorph, Phys. Chem. Chem. Phys. 13 (2011) 14565–14570.
[13] Q. Huang, D. Yu, Z. Zhao, S. Fu, M. Xiong, Q. Wang, Y. Gao, K. Luo, J. He, Y. Tian, First-principles study of O-BN: a sp3-bonding boron nitride allotrope, J. Appl. Phys. 112 (2012) 053518.
[14] C. He, L. Sun, C. Zhang, X. Peng, K. Zhang, J. Zhong, Z-BN: a novel superhard boron nitride phase, Phys. Chem. Chem. Phys. 14 (2012) 10967–10971.
[15] X. Jiang, J. Zhao, R. Ahuja, A novel superhard BN allotrope under cold compression of h-BN, J. Phys. Condens. Matter 25 (2013) 122204.
[16] J. Dai, X. Wu, J. Yang, X.C. Zeng, Porous boron nitride with tunable pore size, J. Phys. Chem. Lett. 5 (2014) 393–398.
[17] A.A. Kuzubov, L.V. Tikhonova, A.S. Fedorov, Ab initio investigation of a new boron nitride allotrope, Phys. Status Solidi B 251 (2014) 1282–1285.
[18] M. Xiong, C. Fan, Z. Zhao, Q. Wang, J. He, D. Yu, Z. Liu, B. Xu, Y. Tian, Novel three-dimensional boron nitride allotropes from compressed nanotube bundles, J. Mater. Chem. C 2 (2014) 7022–7028.
[19] N. Xu, J.F. Li, B.L. Huang, B.L. Wang, Polycrystalline boron nitride constructed from hexagonal boron nitride, RSC Adv. 4 (2014) 38589–38593.
[20] Z. Zhang, M. Lu, L. Zhu, L. Zhu, Y. Li, M. Zhang, Q. Li, Orthorhombic BN: a novel superhard boron nitride allotrope, Phys. Lett. A 378 (2014) 741–744.
[21] J. Long, C. Shu, L. Yang, M. Yang, Predicting crystal structures and physical properties of novel superhard p-BN under pressure via first-principles investigation, J. Alloy. Compd. 644 (2015) 638–644.
[22] Z. Ma, Z. Han, X. Liu, X. Yu, D. Wang, Y. Tian, Pnma-BN: another boron nitride polymorph with interesting physical properties, Nanomaterials 7 (2016) 3.
[23] X.-Y. Ren, C.-X. Zhao, C.-Y. Niu, J.-Q. Wang, Y. Jia, J.-H. Cho, First-principles study of the crystal structures and physical properties of H18-BN and Rh6-BN, Phys. Lett. A 380 (2016) 3891–3896.
[24] P. Gao, X. Chen, L. Guo, Z. Wu, E. Zhang, B. Gong, Y. Zhang, S. Zhang, BN-schwarzite: novel boron nitride spongy crystals, Phys. Chem. Chem. Phys. 19 (2017) 1167–1173.
[25] R. Zhou, J. Dai, X. Cheng Zeng, Structural, electronic and mechanical properties of sp3-hybridized BN phases, Phys. Chem. Chem. Phys. 19 (2017) 9923–9933.
[26] É. Germaneau, G. Su, Q.-R. Zheng, New boron nitride structures B4N4: a first-principles random searching application, J. Phys. Condens. Matter 25 (2013) 125504.
[27] G. Yang, B.F. Chen, Predicted a novel high-pressure superhard boron nitride phase, J. Alloy. Compd. 598 (2014) 54–56.
[28] C.-Y. Niu, J.-T. Wang, Three-dimensional three-connected tetragonal BN: ab initio calculations, Phys. Lett. A 378 (2014) 2303–2307.
[29] S. Zhang, Q. Wang, Y. Kawazoe, P. Jena, Three-dimensional metallic boron nitride, J. Am. Chem. Soc. 135 (2013) 18216–18221.
[30] J. Dai, X. Wu, J. Yang, X.C. Zeng, Unusual metallic microporous boron nitride networks, J. Phys. Chem. Lett. 4 (2013) 3484–3488.
[31] M. Xiong, K. Luo, D. Yu, Z. Zhao, J. He, G. Gao, Pressure-induced boron nitride nanotube derivatives: 3D metastable allotropes, J. Appl. Phys. 121 (2017) 165106.
[32] Y. Li, J. Hao, H. Liu, S. Lu, J.S. Tse, High-energy density and superhard nitrogen-rich B-N compounds, Phys. Rev. Lett. 115 (2015) 105502.
[33] S. Zhao, J. Long, Theoretical investigation of the electronic structure, optical, elastic and thermodynamics properties of a newly binary boron nitride (T-B3N3), Phys. B: Condens. Matter 459 (2015) 134–139.
[34] A. Rubio, J.L. Corkill, M.L. Cohen, Theory of graphitic boron nitride nanotubes, Phys. Rev. B 49 (1994) 5081–5084.
[35] N.G. Chopra, R.J. Luyken, K. Cherrey, V.H. Crespi, Boron nitride nanotubes, Science 269 (1995) 966–967.
[36] Y. Wang, J. Lv, L. Zhu, Y. Ma, Crystal structure prediction via particle-swarm optimization, Phys. Rev. B 82 (2010) 094116.
[37] S.J. Clark, M.D. Segall, C.J. Pickard, P.J. Hasnip, M.I.J. Probert, K. Refson, M.C. Payne, First principles methods using CASTEP, Z. Kristallogr. 220 (2005) 567–570.
[38] D.R. Hamann, M. Schlüter, C. Chiang, Norm-conserving pseudopotentials, Phys. Rev. Lett. 43 (1979) 1494.
[39] D.M. Ceperley, B.J. Alder, Ground state of the electron gas by a stochastic method, Phys. Rev. Lett. 45 (1980) 566.
[40] J.P. Perdew, A. Zunger, Self-interaction correction to density-functional approximations for many-electron systems, Phys. Rev. B 23 (1981) 5048.
[41] H.J. Monkhorst, J.D. Pack, Special points for Brillouin-zone integrations, Phys. Rev. B 13 (1976) 5188.
[42] J. Heyd, G.E. Scuseria, M. Ernzerhof, Hybrid functionals based on a screened Coulomb potential, J. Chem. Phys. 118 (2003) 8207–8215.
[43] G. Kresse, J. Furthmüller, Efficient iterative schemes for ab initio total-energy calculations using a plane-wave basis set, Phys. Rev. B 54 (1996) 11169.
[44] Z.-j. Wu, E.-j. Zhao, H.-p. Xiang, X.-f. Hao, X.-j. Liu, J. Meng, Crystal structures and elastic properties of superhardIrN2andIrN3from first principles, Phys. Rev. B 76 (2007) 054115.
[45] X. Guo, L. Li, Z. Liu, D. Yu, J. He, R. Liu, B. Xu, Y. Tian, H.-T. Wang, Hardness of covalent compounds: roles of metallic component and d valence electrons, J. Appl. Phys. 104 (2008) 023503.
[46] X.-Q. Chen, H. Niu, D. Li, Y. Li, Modeling hardness of polycrystalline materials and bulk metallic glasses, Intermetallics 19 (2011) 1275–1281.